BIOCHEMISTRY
including biophysical chemistry & molecular biology

Article

pubs.acs.org/biochemistry

Structural Insights into the Interaction between the Bacterial Flagellar Motor Proteins FliF and FliG

Robert Levenson, Hongjun Zhou, and Frederick W. Dahlquist*

Department of Chemistry and Biochemistry, University of California, Santa Barbara, California 93106-9510, United States

Supporting Information

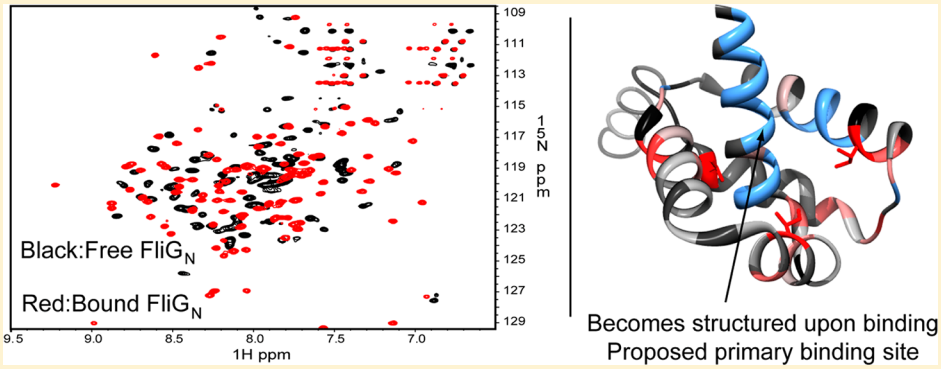

ABSTRACT: The binding of the soluble cytoplasmic protein FliG to the transmembrane protein FliF is one of the first interactions in the assembly of the bacterial flagellum. Once established, this interaction is integral in keeping the flagellar cytoplasmic ring, responsible for both transmission of torque and control of the rotational direction of the flagellum, anchored to the central transmembrane ring on which the flagellum is assembled. Here we isolate and characterize the interaction between the N-terminal domain of *Thermotoga maritima* FliG (FliG$_N$) and peptides corresponding to the conserved C-terminal portion of *T. maritima* FliF. Using nuclear magnetic resonance (NMR) and other techniques, we show that the last ∼40 amino acids of FliF (FliF$_C$) interact strongly (upper bound K_d in the low nanomolar range) with FliG$_N$. The formation of this complex causes extensive conformational changes in FliG$_N$. We find that *T. maritima* FliG$_N$ is homodimeric in the absence of the FliF$_C$ peptide but forms a heterodimeric complex with the peptide, and we show that this same change in oligomeric state occurs in full-length *T. maritima* FliG, as well. We relate previously observed phenotypic effects of FliF$_C$ mutations to our direct observation of binding. Lastly, on the basis of NMR data, we propose that the primary interaction site for FliF$_C$ is located on a conserved hydrophobic patch centered along helix 1 of FliG$_N$. These results provide new detailed information about the bacterial flagellar motor and support efforts to understand the cytoplasmic ring's precise molecular structure and mechanism of rotational switching.

Directed bacterial motility is driven by the regulation of the rotational direction of the bacteria's flagella. Flagella alternate between clockwise and counterclockwise rotation, propelling the bacteria toward optimal environments through a "biased random walk" mechanism.[1,2] The flagellum can be considered as being assembled upon an inner membrane ring (the MS-ring) composed of ∼26 copies[3] of the transmembrane protein FliF. Torque to rotate the flagellar motor is generated by peptidoglycan-anchored membrane protein complexes composed of two proteins, MotA and MotB, which encircle the rotating motor. Both transmission of torque from the Mot proteins and control of the rotational direction of the motor ("switching") rely on a ring of proteins at the cytoplasmic face of the flagellum called the C-ring. The C-ring is composed of three proteins with differing copy numbers: FliG (∼26 copies per ring),[4] FliM (∼34 copies),[5,6] and FliN (110−140 copies).[7,8] FliG is an entirely α-helical protein composed of three domains connected by linkers. The first ∼90 amino acids (in *Thermotoga maritima*) of FliG form the N-terminal domain, FliG$_N$, which interacts with FliF and is discussed in greater detail below. The other two domains of FliG, FliG$_M$ (residues ∼110−190) and FliG$_C$ (residues ∼195−335), have been implicated in both assembly and switching of the motor.[9,10] FliG$_C$ is thought to form the direct torque-generating interactions with the Mot proteins through a series of charged residues located along a ridge in the domain.[11] FliM has been shown to be critical for switching[12] and has been shown both in vitro and in vivo to form interactions with both FliG$_M$ and FliG$_C$.[13] The exact roles of these interactions remain under intense investigation.[14−17] FliN, which exists in an approximately 4:1 ratio to FliM, is thought to assemble in a pseudosymmetric tetrameric ring and interact with the C-terminal domain of FliM, and has been implicated in both assembly and switching of the flagellum.[18,19]

Received: April 10, 2012
Revised: June 6, 2012
Published: June 6, 2012

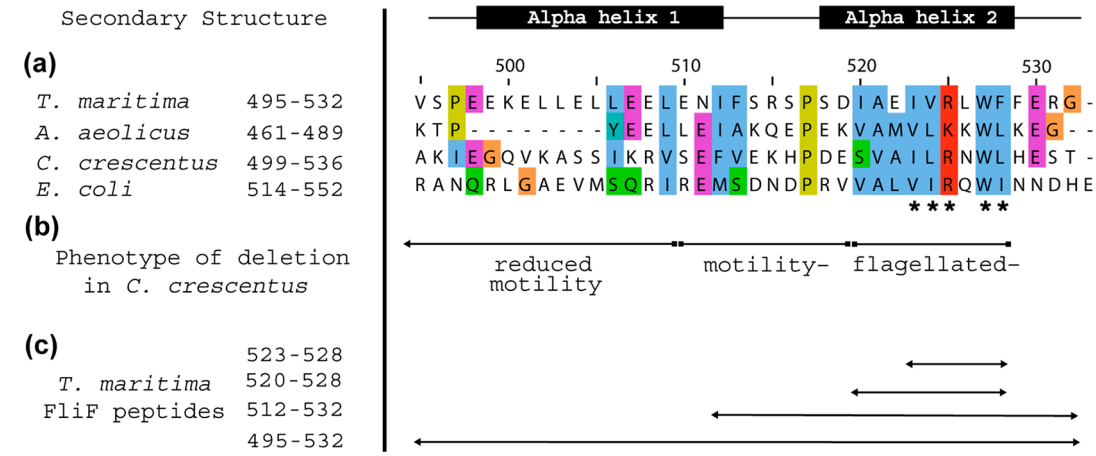

Figure 1. Sequence alignments, phenotypes of mutations, and $FliF_C$ peptides used in this report. (a) Multiple-sequence alignment of the cytoplasmic C-terminal segment of FliF. The predicted secondary structure is shown above the sequences. The most conserved amino acids in α-helix 2, determined from analysis of a larger set of sequences, are marked with stars. Sequence numbers in the respective organisms are shown next to the organism's name. Alignment was performed using ClustalX.[41] The multiple-sequence alignment image was made in Jalview[42] and colored according to the default ClustalX scheme. (b) Phenotypes of *C. crescentus* mutants[27] with deleted segments in the indicated ranges. "Flagellated" mutants did not have visible flagellation. "Motility" mutants, while flagellated, did not show motility on soft agar plates. (c) Portions of $FliF_C$ represented by the synthetic peptides that were tested in this paper.

The assembly of the flagellum is thought to begin with the organization of transmembrane protein FliF into the MS-ring.[20] Next, the C-ring is formed around the MS-ring.[21] Because binding of FliG to FliF is essential for C-ring construction, and the C-ring is necessary for assembly of the remainder of the flagellum,[22,23] the interaction between FliF and FliG represents one of the first identified steps in the assembly of the flagellum. Two-hybrid screening,[24] scanning deletions,[9] and the generation of partially motile FliF−FliG fusion proteins[25,26] have indicated that the first ∼50 amino acids of $FliG_N$ are essential for, and thus likely involved in, binding to FliF. An in vivo study using *Caulobacter crescentus* showed that deletions within the last 38 amino acids of FliF (excluding a few residues at the very C-terminus) affect flagellar assembly and bacterial motility, again presumably through their involvement in the interaction of FliF with FliG.[27] These 38 amino acids ($FliF_C$) are well-conserved and are predicted by secondary structure prediction algorithms to form two α-helices (Figure 1a). A highly conserved (residues 520−528 in *T. maritima*) portion of $FliF_C$, including a nearly absolutely conserved tryptophan (W527 in *T. maritima*), was found to be required for assembly (Figure 1b). An extended sequence, including the region just described and including an additional 10 amino acids (residues 510−528, in total, in *T. maritima*), was found to be essential for motility. Lastly, the full 38-amino acid $FliF_C$ sequence (residues 491−528 in *T. maritima*) was identified as being necessary for full wild-type motility. In this study, we have reconstituted the interaction between $FliF_C$ and $FliG_N$ in vitro and have used a combination of NMR and other techniques to characterize their binding.

MATERIALS AND METHODS

Protein Purification. *T. maritima* $FliG_N$ constructs were generated from a $FliG_{NM}$ construct encoded on vector pJY5 provided by D. Blair (University of Utah, Salt Lake City, UT), with an N-terminal eight-His tag and a TEV protease site. The $FliG_N$ constructs were created by introducing stop codons at appropriate sites. Constructs were confirmed by DNA sequencing.

All proteins were expressed in BL21-Rosetta cells grown at 37 °C. Cells grown in LB medium were induced with 1 mM IPTG at an OD_{600} of ∼0.5, followed by a 6 h expression after which cells were pelleted and frozen at −80 °C for later use. Isotopically enriched proteins were grown in M9 medium from starter cultures in LB using standard methods. Briefly, pelleted cells from overnight cultures of cells grown in LB were added to M9 minimal medium containing [^{15}N]ammonium chloride, with [^{13}C]glucose and/or D_2O when appropriate. After recovery had been allowed, cells were induced at an OD_{600} of ∼0.4 and allowed to express overnight before being harvested.

$FliG_N$ protein, after cell lysis and a 10 min heat shock at ∼70 °C, was purified by nickel-affinity chromatography. Column-bound $FliG_N$ was washed with 130 mM imidazole, followed by elution from the column with 250 mM imidazole. $FliG_N$ was further purified by size-exclusion fast performance liquid chromatography, providing pure protein as shown on sodium dodecyl sulfate−polyacrylamide gel electrophoresis (SDS−PAGE) gels. The purified protein was then concentrated and stored at 4 °C or frozen at −80 °C until it was used. The final buffer used for NMR and fluorescence experiments consisted of 50 mM sodium phosphate, 100 mM NaCl, and 0.5 mM EDTA (pH 6.5).

The DNA sequence encoding *T. maritima* full-length $FliG_{NMC}$ was obtained from the Joint Center for Structural Genomics (JCSG). The $FliG_{NMC}$ sequence, including an N-terminal six-His tag, was then subcloned into the pET-22b vector. Purification and buffer conditions were as described above, except $FliG_{NMC}$ was washed with 30 mM instead of 130 mM imidazole.

When the reaction was performed, the N-terminal His tag on $FliG_N$ was excised using AcTEV protease (Invitrogen). Digestion was performed at 30 °C until completion, using SDS−PAGE analysis for confirmation of cleavage.

Synthetic $FliF_C$ Peptides. Synthetic $FliF_{495-532}$ peptide (∼90% pure) was obtained from EZ Biolab or NEO BioScience. Synthetic $FliF_{512-532}$, $FliF_{520-528}$, and $FliF_{523-528}$ peptides (∼80% pure) were obtained from Biomatik Corp.

dx.doi.org/10.1021/bi3004582 | *Biochemistry* 2012, 51, 5052−5060

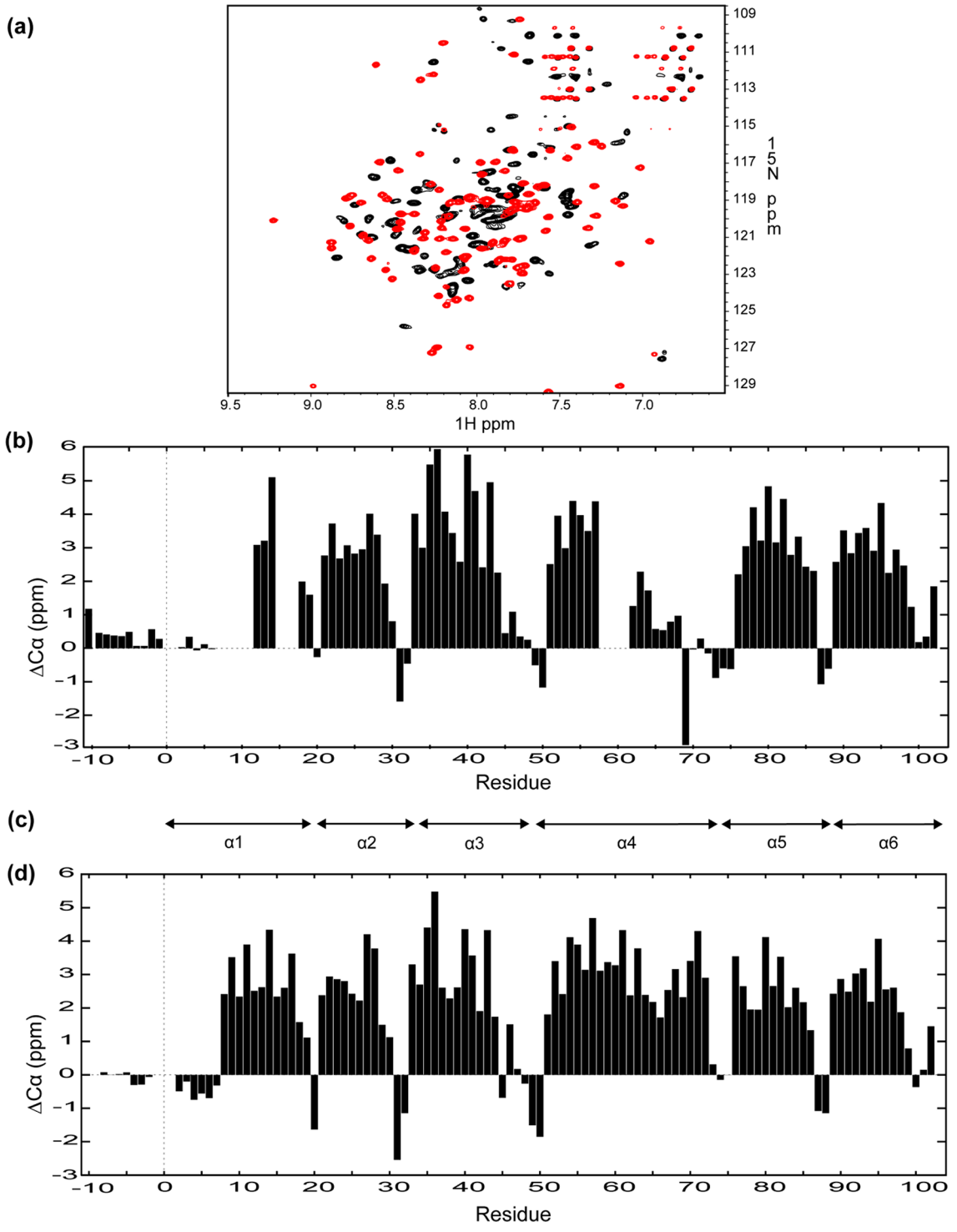

Figure 2. NMR data from $FliG_N$ bound and not bound to $FliF_{495-532}$. (a) Overlay of $^1H-^{15}N$ TROSY-HSQC spectra of $[^{15}N,^2H]FliG_N$ (black) and $[^{15}N,^2H]FliG_N$ with $FliF_{495-532}$ (red). (b) Cα chemical shift deviations from random coil values in free $FliG_N$. (c) Locations of α-helices in $FliG_N$, as observed in the *A. aeolicus* crystal structure and from computational predictions. (d) Cα chemical shift deviations from random coil values in $FliG_N$ bound to $FliF_{495-532}$.

For use in experiments, lyophilized peptide was dissolved in final buffer and then adjusted to the appropriate pH.

NMR Spectroscopy. NMR experiments were performed on either a Varian Inova 600 MHz or a Bruker Avance III Ultrashield Plus 800 MHz spectrometer. All experiments were performed at 40 °C with 8% (v/v) D_2O added to buffer. Initial assignments of $FliG_N$ were made using HNCACB[28,29] and CBCA(CO)NH[29,30] pulse sequences with an ~0.5 mM ^{15}N- and ^{13}C-labeled $FliG_N$ sample. Later confirmation of $FliG_N$ assignments and the assignments of ^{15}N-, ^{13}C-, and ^2H-labeled $FliG_N$ bound to unlabeled $FliF_{495-532}$ was performed using HNCA, HNCACB, HN(CO)CA, and HN(CO)CACB sequences.[29,31,32] Binding between labeled $FliG_N$ and peptides was observed using $^1H-^{15}N$ HSQC and $^1H-^{15}N$ TROSY-HSQC pulse sequences. NMR data were processed using

dx.doi.org/10.1021/bi3004582 | *Biochemistry* 2012, 51, 5052−5060

nmrPipe,[33] and assignments were performed with a modified version of ANSIG.[34]

Chemical shift assignments have been deposited in the BioMagResBank as entries 18309 ($FliG_N$) and 18310 (labeled $FliG_N$ bound to unlabeled $FliF_{495-532}$).

Fluorescence Spectroscopy. $FliG_N$ was purified to homogeneity before analysis. The synthetic peptide was prepared at appropriate concentrations as described above. The concentration of the peptide was determined using absorption of UV light at 280 nm (ε = 5500 M^{-1} cm^{-1}). Each step in the shown titrations was measured 10 times and averaged. Titrations were repeated at least twice. Fluorescence analysis was performed using a Perkin-Elmer LS 55 fluorimeter and analyzed using FL WinLab.

Size-Exclusion Chromatography and Light Scattering. Size-exclusion chromatography with static light scattering analysis was performed using a system consisting of a Wyatt Technologies Minidawn TREOS multiangle light scattering detector, a Wyatt Technologies t-rEX refractive index detector, a Waters UV detector, and an HPLC pump, with proteins separated on Wyatt Technologies HPLC size-exclusion columns. Purified individual proteins or protein complexes were run at ~1 mg/mL. Wyatt Technologies ASTRA software was used for analysis and molecular weight determination. Size-exclusion chromatography–light scattering experiments were performed in 25 mM Tris, 200 mM NaCl, and 0.5 mM EDTA (pH 7.4).

RESULTS

All the experiments in this work were performed with proteins from *T. maritima*, a monotrichously flagellated thermophile originally harvested from thermal vents.[35] Proteins from *T. maritima* have been used in many structural studies of the flagellar C-ring, and crystal structures of $FliG_{MC}$,[10] the N-domain and middle domains of FliM,[36] and most of FliN[8] now exist. More recently, the crystal structure of full-length FliG from *Aquifex aeolicus* was determined, providing the first structure of the $FliG_N$ domain,[15] although in the absence of FliF. There is good sequence conservation of FliG among *Escherichia coli*, *T. maritima*, *A. aeolicus*, and *C. crescentus*, so it likely that the general structure and mechanism of torque transmission of FliG is conserved among organisms. To facilitate NMR studies and to isolate the interaction of interest, we generated or obtained smaller protein constructs of FliG and FliF, respectively. On the FliG side, multiple $FliG_N$ constructs were derived from a *T. maritima* $FliG_{NM}$ construct generously provided by D. Blair. $FliG_N$ protein constructs encoding residues 1–52, 1–73, and 1–89 of FliG were found to be unfolded, as judged by analysis of one-dimensional proton NMR and/or $^1H-^{15}N$ correlated spectroscopy using ^{15}N-enriched purified protein (data not shown). A construct encoding residues 1–102, which includes the entire $FliG_N$ domain and approximately one-half of the α-helix linker that connects $FliG_N$ to $FliG_M$, was found to be stable and had moderately well-dispersed peaks (Figure 2a, black). This construct, which includes an N-terminal eight-His tag along with a TEV protease site, was used for the rest of this study and will be termed simply $FliG_N$. Removal of the affinity tag was found to have no significant effects on the NMR spectra of labeled $FliG_N$, so all data shown here were for $FliG_N$ with the His tag attached.

NMR Characterization of $FliG_N$ and $FliF_C$ Peptide Binding. Using triply labeled (^{15}N, ^{13}C, and ^2H) protein, $FliG_N$ resonances were assigned using standard three-dimensional (3D) NMR techniques. Analysis of Cα secondary shifts from random coil values indicates a six-helix protein (Figure 2b), in agreement with the published crystal structure of $FliG_N$ from *A. aeolicus* FliG and computational secondary structure predictions (Figure 2c).[37,38] We were able to assign ~86% (excluding affinity tag residues) of the protein backbone amide resonances. Missing resonances were grouped into two regions, composed of residues on helix 1 of $FliG_N$ (amino acids 7–11 and 15–17) and a series of residues on helix 4 (amino acids 58–61). These resonances are likely broadened because of the dynamic properties of the residues, indicating a lack of structural rigidity in these areas. Helix 1 forms the central helix around which the rest of the domain is folded, and a lack of stable structure in helix 1 likely leads to increased conformational heterogeneity in the rest of the protein. Notably, the broadened resonances corresponding to amino acids 15–17 are located in the center of a highly conserved row of hydrophobic residues in the $FliG_N$ sequence (Figure S1 of the Supporting Information). While examination of the crystal structure of $FliG_N$ from *A. aeolicus* shows that some of these residues are buried in the core of the domain, others are completely or partially solvent exposed. Residues 58–61 of helix 4, also not detected because of resonance broadening, are located immediately next to helix 1 in the crystal structure of $FliG_N$, further indicating instability in the region surrounding the central helix. The lack of structure in this area of helix 4 propagates through to the helix 4–helix 5 turn.

As discussed above, an earlier in vivo study using *C. crescentus* showed that deletions of different portions of $FliF_C$ caused varying phenotypic effects. To examine these effects, we purchased synthetic peptides from commercial sources corresponding to four selected portions of $FliF_C$, which we used to probe for an interaction with $FliG_N$ (Figure 1c). These peptides correspond to the regions necessary in vivo for flagellar assembly (peptides $FliF_{520-528}$ and $FliF_{523-528}$), the region necessary for motility ($FliF_{512-532}$, covering only helix 2 of $FliF_C$), and the region necessary for wild-type motility ($FliF_{495-532}$, including both helices 1 and 2 of $FliF_C$). We then tested for interactions between these peptides and [^{15}N,^2H]-$FliG_N$ using $^1H-^{15}N$ TROSY-HSQC experiments. As the synthetic peptides were not enriched with NMR-visible isotopes, all the NMR analysis was performed from the perspective of the labeled $FliG_N$ and does not provide direct information about the structure or conformational changes of the $FliF_C$ peptides.

We observed no shifts in the spectrum of $FliG_N$ when it was mixed with large excesses of peptides $FliF_{520-528}$ and $FliF_{523-528}$, suggesting that these smaller peptides do not interact with $FliG_N$. Both larger peptides did bind $FliG_N$ and caused widespread perturbations across the spectrum, indicating large conformational changes in $FliG_N$. Shifts in $FliG_N$ upon peptide binding were notably different between $FliF_{495-532}$ and $FliF_{512-532}$. Binding of $FliF_{495-532}$ to $FliG_N$ is shown in Figure 2a (red). Binding of $FliF_{512-532}$ is compared with binding of $FliF_{495-532}$ and the unbound $FliG_N$ spectrum in Figure S2a of the Supporting Information. Although the overall $FliG_N$ chemical shift perturbations from the two peptides are comparable in magnitude and direction, which shows that the general mode of binding is similar, few resonances in the bound spectra overlay. The spectrum of $FliG_N$ bound to $FliF_{512-532}$ is not intermediate between those of unbound $FliG_N$ and $FliG_N$ bound to $FliF_{495-532}$. Instead, the differences between the

dx.doi.org/10.1021/bi3004582 | *Biochemistry* 2012, 51, 5052–5060

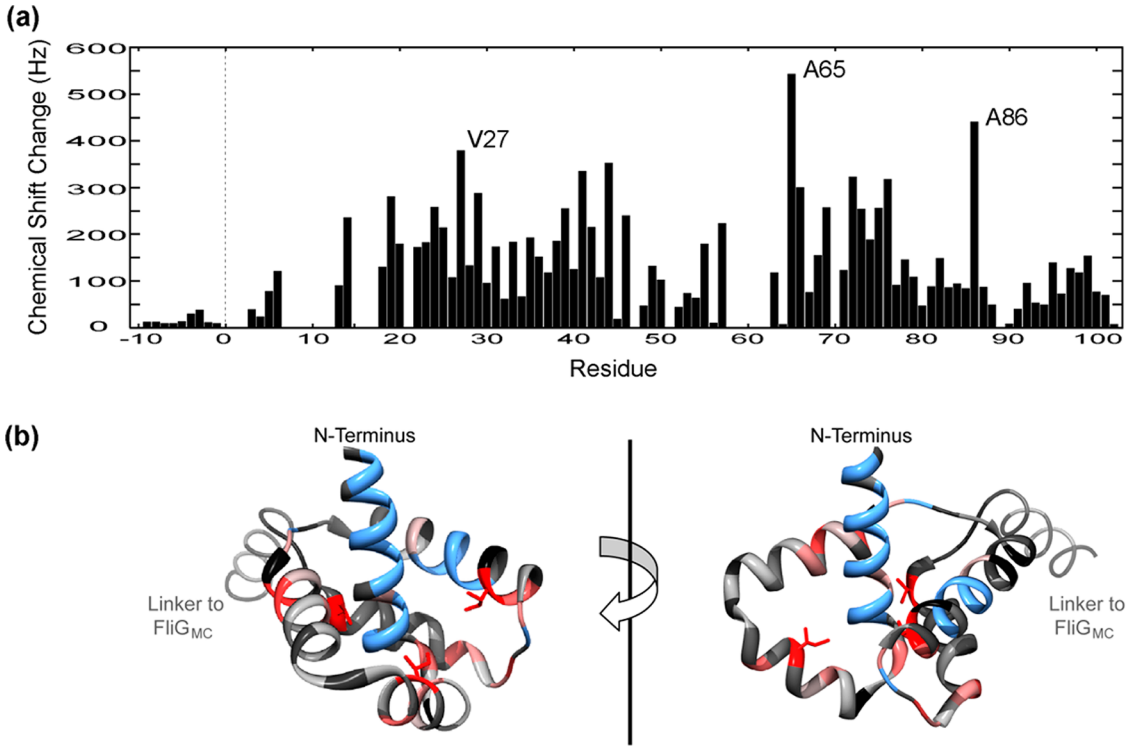

Figure 3. Chemical shift perturbations in $FliG_N$ upon $FliF_{495-532}$ binding. (a) Chemical shift perturbations to amide $^{15}N-^{1}H$ resonances upon addition of $FliF_{495-532}$ to ^{15}N- and ^{2}H-labeled $FliG_N$. The shifts are shown as absolute values. (b) Chemical shift perturbations from the NMR titration mapped onto the crystal structure of *A. aeolicus* $FliG_N$. The relative sizes of shifts increase in the following order: black < gray < red. Blue denotes residues for which a change cannot be mapped because of a lack of assignment in either the bound or unbound state, almost all due to missing residues in unbound $FliG_N$. The residues with the largest shifts are shown as sticks (corresponding in *T. maritima* to A86, A65, and V27, in clockwise order starting from the top left red residue on the left side). The protein image was created using UCSF Chimera.[43]

spectra of $FliG_N$ bound to the two peptides indicate that α-helix 1 of $FliF_C$ plays an important structural role in $FliG_N$ binding. This implies that the contact interface between FliF and $FliG_N$ is widespread across both helices 1 and 2 of the $FliF_C$ peptide. Because the $FliF_{512-532}$ peptide could not reproduce the interaction of the larger $FliF_{495-532}$ peptide (in addition to poor solubility), we chose to use $FliF_{495-532}$ for further characterization.

Binding of $FliF_{495-532}$ to $FliG_N$. Because binding to $FliF_{495-532}$ (as well as $FliF_{512-532}$) occurred in the slow-exchange regime, 3D NMR experiments were used to assign the resonances of $FliG_N$ when it was in complex with the peptide; ~99% of the $FliF_{495-532}$-bound $FliG_N$ backbone amide resonances were assigned. Relative to that of unbound $FliG_N$, the spectrum of $FliG_N$ bound to the $FliF_{495-532}$ peptide was much sharper and had better dispersion of peaks. Cα secondary shifts show that the secondary structure of $FliG_N$ bound to $FliF_{495-532}$ is similar overall to that of unbound $FliG_N$ (Figure 2d). However, the regions of $FliG_N$ that were missing resonances and likely unstructured in the absence of $FliF_{495-532}$ were found to be easily assignable in the peptide-bound state and to now possess significant secondary structure. This likely reflects a large reduction in the level of conformational exchange for these residues. Both helices 1 and 4, which had little structure in unbound $FliG_N$, have strong α-helical structure when bound to $FliF_{495-532}$. Changes in the chemical shifts of *T. maritima* $FliG_N$ upon binding $FliF_{495-532}$ (Figure 3a) are shown mapped onto the crystal structure of *A. aeolicus* $FliG_N$ (Figure 3b). The three resonances showing the largest chemical shift perturbations upon peptide binding are V27, A65, and A86 (all in *T. maritima* numbering), all partially buried hydrophobic amino acids oriented toward the central helix 1 of $FliG_N$. Large chemical shift perturbations are distributed across the first ~80 amino acids of $FliG_N$, covering helices 1−4. Helices 5 and 6 have relatively smaller perturbations, with the exception of A86, indicating that they are more distant from the interaction site. Because of the widespread changes in chemical shifts across the domain, it is not possible to determine a precise binding site for the peptide directly from chemical shift perturbation mapping. Altogether, the data indicate that the interaction between $FliF_{495-532}$ and $FliG_N$ is extensive and that the interaction between $FliF_C$ and $FliG_N$ likely causes large propagated conformational changes and provides significant stability to the N-terminal domain of FliG.

Characterization of FliG−$FliF_C$ Complexes by Size-Exclusion Chromatography with Light Scattering. We noted while performing NMR experiments that the resonances of $FliG_N$ were broader than expected for its predicted monomeric size (predicted $M_w \approx 13.9$ kDa), and that binding of $FliG_N$ to the peptide led to an unexpectedly large increase in the sharpness of peaks. We thus used a size-exclusion chromatography−light scattering−refractive index system to characterize the oligomeric state of $FliG_N$ alone and in complex with $FliF_{495-532}$. We found that *T. maritima* $FliG_N$ forms a tight homodimer in the absence of peptide (calculated $M_w \approx 31$ kDa), while $FliG_N$ bound to $FliF_{495-532}$ forms a heterodimeric complex (calculated $M_w \approx 17$ kDa) (Figure 4a). Both complexes have very similar retention times on size-exclusion columns despite an ~10 kDa difference in molecular weight,

dx.doi.org/10.1021/bi3004582 | *Biochemistry* 2012, 51, 5052−5060

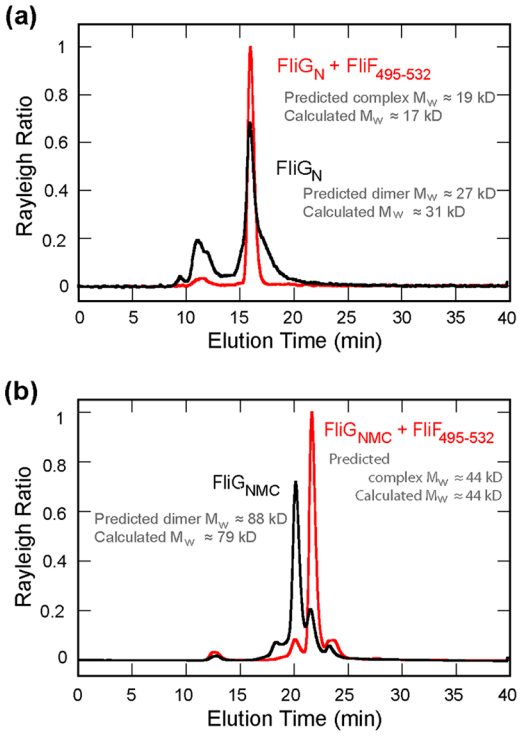

Figure 4. Size-exclusion chromatography–light scattering analysis of FliG constructs with and without $FliF_{495-532}$. (a) Chromatogram of the light scattering signal of *T. maritima* $FliG_N$ with or without the $FliF_{495-532}$ peptide. (b) Chromatogram of the light scattering signal of full-length *T. maritima* $FliG_{NMC}$ with or without the $FliF_{495-532}$ peptide.

possibly because of the cylindrical shape of the $FliG_N$ construct used in these experiments. This indicates that the dimeric interface should occur along the longer cylindrical surface of the protein instead of on either of the cylinder's bases, which would be expected to cause a larger change in retention time. Despite the similar retention times, the oligomeric forms of the different complexes are clearly differentiated by the experimental setup because of the protein concentration calibration from the refractive index detector. To see if these results apply to the full FliG protein as well, we obtained a construct encoding full-length *T. maritima* FliG. Like $FliG_N$, purified full-length FliG forms a tight dimer in the absence of peptide (calculated $M_w \approx$ 79 kDa) and forms a heterodimeric complex when bound to $FliF_{495-532}$ (calculated $M_w \approx 44$ kDa) (Figure 4b). In this case, a difference in retention time is clearly observed. Because the middle and C-terminal domains of FliG do not oligomerize (data not shown), this dimerization of free FliG must be driven by the $FliG_N$ domain.

Fluorescence Analysis of Peptide Binding. $FliF_C$ contains a nearly absolutely conserved tryptophan residue (W527 in *T. maritima*). We therefore monitored the intrinsic fluorescence of W527 in $FliF_{495-532}$, the only tryptophan present in both *T. maritima* $FliF_C$ and $FliG_N$, as a function of $FliG_N$ to probe binding. Addition of $FliG_N$ to the peptide led to an ~4-fold increase in the apparent quantum yield as well as an ~10 nm blue shift in the emission maximum of the tryptophan (Figure 5a,b). Both effects indicate that W527 moves from a solvated to an unsolvated environment when interacting with $FliG_N$. The stoichiometry of binding was one $FliF_C$ peptide to one subunit of $FliG_N$, in line with experiments indicating a 1:1 ratio of FliF to FliG in the flagellar motor.[26] The affinity of

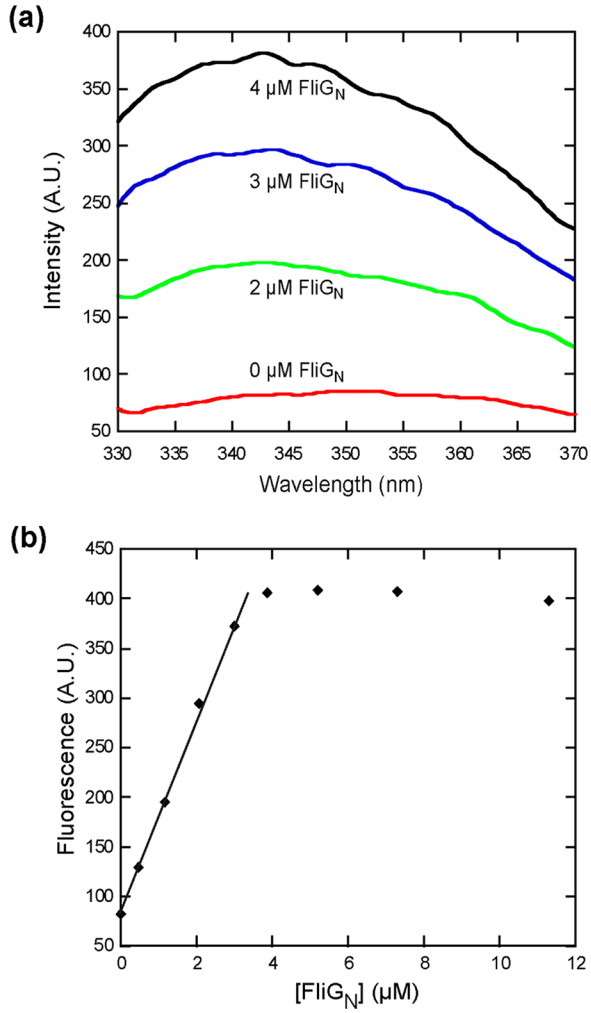

Figure 5. Changes in fluorescence from W527 in $FliF_C$ upon $FliG_N$ binding. (a) Fluorescence spectrum from 330 to 370 nm of a titration of ~4 μM $FliF_C$ peptide with $FliG_N$. (b) Fluorescence intensity (λ_{ex} = 295 nm, and λ_{em} = 352 nm) of another titration of ~4 μM $FliF_{495-532}$ peptide with $FliG_N$.

$FliF_{495-532}$ was too strong to be measured by the fluorescence assay; binding was stoichiometric within the usable range of the fluorescence signal [lowest interpretable measurement using ~40 nM $FliF_{495-532}$ (data not shown)]. We therefore estimate an upper bound for the dissociation constant in the low nanomolar range, though the affinity may indeed be significantly stronger than that. We also measured the affinity of the shorter $FliF_{512-532}$ for $FliG_N$ using the same fluorescence assay. From the binding curve, we measured a K_d of ~84 nM (Figure S2b of the Supporting Information), demonstrating that although there is strong binding between $FliF_{512-532}$ and $FliG_N$, the shorter peptide interacts at least 1 order of magnitude more weakly with $FliG_N$ than $FliF_{495-532}$ does.

DISCUSSION

In this study, we have reconstituted and characterized in vitro the interaction between the C-terminal region of FliF and the N-terminal region of FliG ($FliG_N$). Previous in vivo work with *C. crescentus* has shown that a relatively small series of residues located at the C-terminus of FliF ($FliF_C$) are necessary for flagellar assembly and has noted distinct phenotypic effects for particular deletion mutations in this region. In particular,

dx.doi.org/10.1021/bi3004582 | *Biochemistry* 2012, 51, 5052–5060

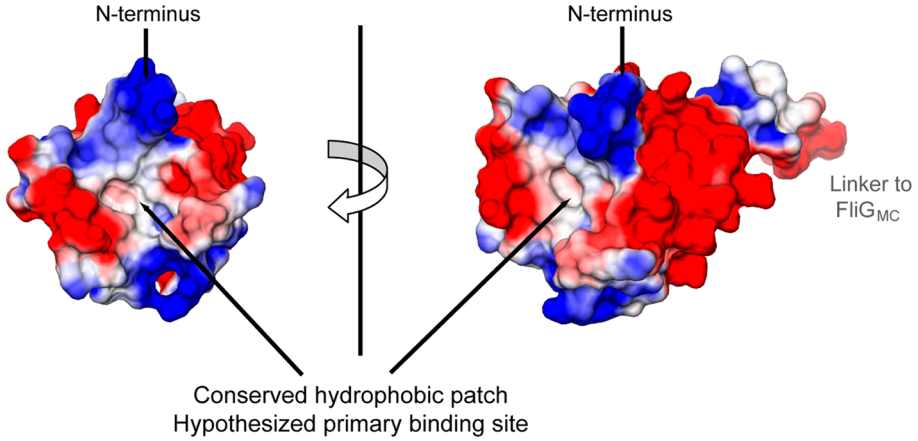

Figure 6. Poisson−Boltzmann electrostatic surface map of *A. aeolicus* FliG$_N$. Blue represents negative surface, red positive surface, and white neutral surface. Electrostatic field generated using the APBS[44] plugin for PyMOL. Image rendered using UCSF Chimera.

analysis has identified one region necessary for flagellar assembly, a larger region necessary for motility, and a yet larger area necessary for wild-type motility. We investigated the interaction between these proteins directly by obtaining synthetic peptides corresponding to these regions. Our data correlate the phenotypic effects of the in vivo mutants with differences in the binding between our FliF$_C$ peptides and FliG$_N$ in vitro. We observed that minimal peptides corresponding to the most highly conserved regions of FliF$_C$ are not sufficient in themselves to ensure binding. However, the large increase in the apparent quantum yield of the highly conserved W527 in FliF$_{495-532}$ upon FliG$_N$ binding indicates that this region is certainly directly involved in binding when it is part of a larger peptide. One explanation for this disparity may be that the shorter FliF$_{520-528}$ and FliF$_{523-528}$ peptides are not sufficiently folded to form the necessary interactions with FliG$_N$. Observation of an upfield methyl ^{1}H peak in FliF$_{512-532}$ and FliF$_{495-532}$, but not in the shorter peptides (data not shown), suggests that the longer peptides have some structure while the shorter ones do not. Differences in the chemical shift perturbations of FliG$_N$ backbone resonances upon binding FliF$_{512-532}$ or FliF$_{495-532}$ indicate that both FliF$_C$ helices 1 and 2 are involved in interactions with FliG$_N$. This conclusion correlates nicely with the in vivo observation that a FliF protein lacking helix 1 of FliF$_C$ is sufficient for flagellar assembly and some motility but cannot support wild-type motility.

The reason for the importance of FliF$_C$ helix 1 in ensuring wild-type motility is unclear. The interaction between FliF and FliG has been previously postulated to be purely structural, based on a lack of isolated switch-biasing mutants in the N-terminal region of FliG, despite attempts at their generation.[39] The second transmembrane segment of FliF is separated from the conserved helices 1 and 2 of FliF$_C$ by ∼35 unconserved amino acids. Though these residues might be expected to provide some flexibility in the positioning of FliF$_C$, it is possible that the observed phenotypic effects of the FliF$_C$ helix 1 deletion mutants are due to either a forced translocation or reorientation of the FliG$_N$ domain, therefore preventing the connected middle and C-terminal domains from assuming their normal arrangements. A FliF−FliG fusion mutant, with some reduced motility,[25] was shown by EM analysis to have altered C-rings, possibly explaining its motility defects.[26] Alternatively, the weakened affinity of a shortened FliF$_C$ for FliG$_N$ might lead to a greater degree of dissociation of FliG from FliF in vivo, which could have effects on motility because this intermolecular interaction is necessary for transmitting the torque from the stators to the body of the flagellum. Photobleaching experiments using a wild-type *E. coli* FliG−GFP fusion showed no fluorescence recovery, indicating that there is normally little or no turnover of FliG in the C-ring.[40] Lastly, it is possible that the correlation of an in vivo motility effect with the observed difference in binding reflects an unidentified role of the FliG$_N$−FliF$_C$ complex in torque conduction or switching, though what that role might be is unknown.

Using fluorescence spectroscopy, we were able to probe binding of FliF$_{495-532}$ to FliG$_N$. As expected, we measured a 1:1 binding stoichiometry between FliF$_C$ and FliG$_N$. We were able to determine an upper bound for the dissociation constant between FliF$_{495-532}$ and FliG$_N$ in the low nanomolar range. The interaction between FliF and FliG has previously shown itself to be very hardy: pH 2.5 conditions are necessary to dissociate FliG from FliF in flagellar basal body extracts.[27] Given that FliG is responsible for transmitting the torque from the Mot proteins to the basal body of the flagellum, it would be expected that this intermolecular interaction is very strong, as keeping these domains together is crucial for normal flagellar function.

We observed that *T. maritima* FliG tightly dimerizes through the FliG$_N$ domain in the absence of FliF$_C$. A ^{15}N- and ^{13}C-edited NOESY[45] of a mixture of ^{15}N- and ^{13}C-labeled FliG$_N$ domains shows that there is a broad interface between subunits on the face of FliG$_N$ formed by helices 2, 3, and 5 (Figure S3a,b of the Supporting Information). The dimer we observe in our experiments is symmetrical, because only one set of peaks is seen in our NMR spectra. Because this dimer disappears upon FliF$_C$ binding, it is likely that peptide binding causes propagated conformational changes that eliminate the dimerization interface between subunits. It is unknown what the biological role, if any, of this dimerization may be. It may play a role in preventing assembly of FliG with FliM−FliN complexes until FliG is associated with FliF, or it may simply stabilize the FliG$_N$ domain until it can bind FliF. FliG from *A. aeolicus* has been reported to be a monomer in solution, and we are not aware of a conclusive determination of the oligomeric state of *E. coli* FliG, though there are implications it may be monomeric as well.[24]

Binding of FliF$_{495-532}$ to FliG$_N$ leads to widespread conformational changes in the FliG$_N$ domain and causes the stabilization of FliG$_N$ helices 1 and 4. These widespread

changes in $FliG_N$ upon $FliF_C$ binding can be explained by a primary binding site located on the highly conserved hydrophobic patch centered along $FliG_N$ helix 1 (Figure 6). In this model, helix 2 of $FliF_C$ directly interacts with central helix 1 of $FliG_N$, propagating conformational changes through and stabilizing the tertiary structure of the $FliG_N$ domain. The stabilization of helix 1 is reflected in the large perturbations of the chemical shifts of $FliG_N$ hydrophobic residues oriented toward the central helix. Deletion mutations have previously shown that the first ~50 amino acids of FliG, encompassing helices 1−3 of $FliG_N$, are necessary for flagellar assembly. Because the interactions between $FliF_C$ and $FliG_N$ are widespread, $FliG_N$ helices 2 and 3 (as well as additional portions of the protein, such as the helix 4−helix 5 loop) may also be involved in secondary interactions with $FliF_C$. Helices 5 and 6 of $FliG_N$, predicted to be most distal from our proposed binding site, are the smallest shifters upon $FliF_C$ binding. This postulated binding site on $FliG_N$ would also provide a very favorable orientation for assembly of the C-ring: the FliF binding site would be directly opposite the linker helix that connects $FliG_N$ to the $FliG_{MC}$ domains. Work to determine an atomic-resolution structure of the $FliG_N$−$FliF_C$ complex is ongoing.

■ ASSOCIATED CONTENT

Supporting Information

Multiple-sequence alignment of $FliG_N$ from *T. maritima*, *A. aeolicus*, *C. crescentus*, and *E. coli* (Figure S1); an overlay of $^{15}N-^{1}H$ TROSY-HSQC spectra of $FliG_N$, $FliG_N$ bound to $FliF_{495-532}$, and $FliG_N$ bound to $FliF_{512-532}$ (Figure S2a) and a fluorescence experiment showing the titration of $FliF_{512-532}$ with $FliG_N$ (Figure S2b); and an overlay of the $^{15}N-^{1}H$ HSQC spectrum of $FliG_N$ with NOEs observed between a mixture of ^{15}N- and ^{13}C-labeled $FliG_N$ (Figure S3a) and mapping of interfacial residues with NOEs onto an *A. aeolicus* structure of $FliG_N$ (Figure S3b). This material is available free of charge via the Internet at http://pubs.acs.org.

■ AUTHOR INFORMATION

Corresponding Author

*Telephone: (805) 893-5326. E-mail: dahlquist@chem.ucsb.edu.

Funding

This work was supported by National Institutes of Health Grant GM59544 to F.W.D.

Notes

The authors declare no competing financial interest.

■ ACKNOWLEDGMENTS

We thank Collin Dyer for suggesting this project, Javin Oza for assistance with fluorescence spectroscopy, Armand Vartanian for helpful discussions and assistance with light scattering, David Blair for providing the $FliG_{NM}$ plasmid, and the JCSG for providing the $FliG_{NMC}$ plasmid.

■ ABBREVIATIONS

NMR, nuclear magnetic resonance; HSQC, heteronuclear single-quantum coherence; TROSY, transverse relaxation-optimized spectroscopy; HPLC, high-performance liquid chromatography.

■ REFERENCES

(1) Berg, H. C. (2003) The rotary motor of bacterial flagella. *Annu. Rev. Biochem. 72*, 19−54.
(2) Sowa, Y., and Berry, R. M. (2008) Bacterial flagellar motor. *Q. Rev. Biophys. 41*, 103−132.
(3) Jones, C. J., Macnab, R. M., Okino, H., and Aizawa, S.-I. (1990) Stoichiometric analysis of the flagellar hook-(basal-body) complex of *Salmonella typhimurium*. *J. Mol. Biol. 212*, 377−387.
(4) Zhao, R., Amsler, C. D., Matsumura, P., and Khan, S. (1996) FliG and FliM distribution in the *Salmonella typhimurium* cell and flagellar basal bodies. *J. Bacteriol. 178*, 258−265.
(5) Thomas, D. R., Morgan, D. G., and DeRosier, D. J. (1999) Rotational symmetry of the C ring and a mechanism for the flagellar rotary motor. *Proc. Natl. Acad. Sci. U.S.A. 96*, 10134−10139.
(6) Thomas, D. R., Francis, N. R., Xu, C., and DeRosier, D. J. (2006) The three-dimensional structure of the flagellar rotor from a clockwise-locked mutant of *Salmonella enterica* serovar Typhimurium. *J. Bacteriol. 188*, 7039−7048.
(7) Zhao, R., Pathak, N., Jaffe, H., Reese, T. S., and Khan, S. (1996) FliN is a major structural protein of the C-ring in the *Salmonella typhimurium* flagellar basal body. *J. Mol. Biol. 261*, 195−208.
(8) Brown, P. N., Mathews, M. A. A., Joss, L. A., Hill, C. P., and Blair, D. F. (2005) Crystal structure of the flagellar rotor protein FliN from *Thermotoga maritima*. *J. Bacteriol. 187*, 2890−2902.
(9) Kihara, M., Miller, G. U., and Macnab, R. M. (2000) Deletion analysis of the flagellar switch protein FliG of *Salmonella*. *J. Bacteriol. 182*, 3022−3028.
(10) Brown, P. N., Hill, C. P., and Blair, D. F. (2002) Crystal structure of the middle and C-terminal domains of the flagellar rotor protein FliG. *EMBO J. 21*, 3225−3234.
(11) Lloyd, S. A., and Blair, D. F. (1997) Charged residues of the rotor protein FliG essential for torque generation in the flagellar motor of *Escherichia coli*. *J. Mol. Biol. 266*, 733−744.
(12) Sockett, H., Yamaguchi, S., Kihara, M., Irikura, V. M., and Macnab, R. M. (1992) Molecular analysis of the flagellar switch protein FliM of *Salmonella typhimurium*. *J. Bacteriol. 174*, 793−806.
(13) Marykwas, D. L., and Berg, H. C. (1996) A mutational analysis of the interaction between FliG and FliM, two components of the flagellar motor of *Escherichia coli*. *J. Bacteriol. 178*, 1289−1294.
(14) Dyer, C. M., Vartanian, A. S., Zhou, H., and Dahlquist, F. W. (2009) A molecular mechanism of bacterial flagellar motor switching. *J. Mol. Biol. 388*, 71−84.
(15) Lee, L. K., Ginsburg, M. A., Crovace, C., Donohoe, M., and Stock, D. (2010) Structure of the torque ring of the flagellar motor and the molecular basis for rotational switching. *Nature 466*, 996−1000.
(16) Paul, K., Gonzalez-Bonet, G., Bilwes, A. M., Crane, B. R., and Blair, D. (2011) Architecture of the flagellar rotor. *EMBO J. 30*, 2962−2971.
(17) Paul, K., Brunstetter, D., Titen, S., and Blair, D. F. (2011) A molecular mechanism of direction switching in the flagellar motor of *Escherichia coli*. *Proc. Natl. Acad. Sci. U.S.A. 108*, 17171−17176.
(18) Paul, K., Harmon, J. G., and Blair, D. F. (2006) Mutational analysis of the flagellar rotor protein FliN: Identification of surfaces important for flagellar assembly and switching. *J. Bacteriol. 188*, 5240−5248.
(19) Sarkar, M. K., Paul, K., and Blair, D. F. (2010) Subunit organization and reversal-associated movements in the flagellar switch of *Escherichia coli*. *J. Biol. Chem. 285*, 675.
(20) Macnab, R. M. (2003) How bacteria assemble flagella. *Annu. Rev. Microbiol. 57*, 77−100.
(21) Minamino, T., and Namba, K. (2004) Self-assembly and type III protein export of the bacterial flagellum. *J. Mol. Microbiol. Biotechnol. 7*, 5−17.
(22) Kubori, T., Shimamoto, N., Yamaguchi, S., Namba, K., and Aizawa, S.-I. (1992) Morphological pathway of flagellar assembly in *Salmonella typhimurium*. *J. Mol. Biol. 226*, 433−446.
(23) González-Pedrajo, B., Minamino, T., Kihara, M., and Namba, K. (2006) Interactions between C ring proteins and export apparatus

components: A possible mechanism for facilitating type III protein export. *Mol. Microbiol. 60*, 984−998.
(24) Marykwas, D. L., Schmidt, S. A., and Berg, H. C. (1996) Interacting components of the flagellar motor of *Escherichia coli* revealed by the two-hybrid system in yeast. *J. Mol. Biol. 256*, 564−576.
(25) Francis, N. R., Irikuvra, V. M., Yamaguchi, S., DeRosier, D. J., and Macnab, R. M. (1992) Localization of the *Salmonella typhimurium* flagellar switch protein FliG to the cytoplasmic M-Ring face of the basal body. *Proc. Natl. Acad. Sci. U.S.A. 89*, 6304−6308.
(26) Thomas, D., Morgan, D. G., and DeRosier, D. J. (2001) Structures of bacterial flagellar motors from two FliF-FliG gene fusion mutants. *J. Bacteriol. 183*, 6404−6412.
(27) Grunenfelder, B., Gehrig, S., and Jenal, U. (2003) Role of the cytoplasmic C terminus of the FliF motor protein in flagellar assembly and rotation. *J. Bacteriol. 185*, 1624−1633.
(28) Wittekind, M., and Mueller, L. (1993) HNCACB, a high-sensitivity 3D NMR experiment to correlate amide-proton and nitrogen resonances with the α- and β-carbon resonances in proteins. *J. Magn. Reson., Ser. B 101*, 201−205.
(29) Muhandiram, D. R., and Kay, L. E. (1994) Gradient-enhanced triple-resonance three-dimensional NMR experiments with improved sensitivity. *J. Magn. Reson., Ser. B 103*, 203−216.
(30) Grzesiek, S., and Bax, A. (1992) Correlating backbone amide and side chain resonances in larger proteins by multiple relayed triple resonance NMR. *J. Am. Chem. Soc. 114*, 6291−6293.
(31) Salzmann, M., Pervushin, K., Wider, G., Senn, H., and Wüthrich, K. (1998) TROSY in triple-resonance experiments: New perspectives for sequential NMR assignment of large proteins. *Proc. Natl. Acad. Sci. U.S.A. 95*, 13585−13590.
(32) Yang, D., and Kay, L. (1999) Improved lineshape and sensitivity in the HNCO-family of triple resonance experiments. *J. Biomol. NMR 14*, 273−276.
(33) Delaglio, F., Grzesiek, S., Vuister, G., Zhu, G., Pfeifer, J., and Bax, A. (1995) NMRPipe: A multidimensional spectral processing system based on UNIX pipes. *J. Biomol. NMR 6*, 277−293.
(34) Kraulis, P. (1989) ANSIG: A program for the assignment of protein ^{1}H 2D NMR spectra by interactive computer graphics. *J. Magn. Reson. 84*, 627−633.
(35) Nelson, K. E., Clayton, R. A., Gill, S. R., Gwinn, M. L., Dodson, R. J., Haft, D. H., Hickey, E. K., Peterson, J. D., Nelson, W. C., Ketchum, K. A., McDonald, L., Utterback, T. R., Malek, J. A., Linher, K. D., Garrett, M. M., Stewart, A. M., Cotton, M. D., Pratt, M. S., Phillips, C. A., Richardson, D., Heidelberg, J., Sutton, G. G., Fleischmann, R. D., Eisen, J. A., White, O., Salzberg, S. L., Smith, H. O., Venter, J. C., and Fraser, C. M. (1999) Evidence for lateral gene transfer between Archaea and Bacteria from genome sequence of *Thermotoga maritima*. *Nature 399*, 323−329.
(36) Park, S.-Y., Lowder, B., Bilwes, A. M., Blair, D. F., and Crane, B. R. (2006) Structure of FliM provides insight into assembly of the switch complex in the bacterial flagella motor. *Proc. Natl. Acad. Sci. U.S.A. 103*, 11886−11891.
(37) Wishart, D., and Sykes, B. (1994) The ^{13}C chemical-shift index: A simple method for the identification of protein secondary structure using ^{13}C chemical-shift data. *J. Biomol. NMR 4*, 171−180.
(38) Wishart, D. S., Sykes, B. D., and Richards, F. M. (1991) Relationship between nuclear magnetic resonance chemical shift and protein secondary structure. *J. Mol. Biol. 222*, 311−333.
(39) Irikura, V. M., Kihara, M., Yamaguchi, S., Sockett, H., and Macnab, R. M. (1993) *Salmonella typhimurium fliG* and *fliN* mutations causing defects in assembly, rotation, and switching of the flagellar motor. *J. Bacteriol. 175*, 802−810.
(40) Fukuoka, H., Inoue, Y., Terasawa, S., Takahashi, H., and Ishijima, A. (2010) Exchange of rotor components in functioning bacterial flagellar motor. *Biochem. Biophys. Res. Commun. 394*, 130−135.
(41) Larkin, M. A., Blackshields, G., Brown, N. P., Chenna, R., McGettigan, P. A., McWilliam, H., Valentin, F., Wallace, I. M., Wilm, A., Lopez, R., Thompson, J. D., Gibson, T. J., and Higgins, D. G. (2007) Clustal W and Clustal X version 2.0. *Bioinformatics 23*, 2947−2948.
(42) Waterhouse, A. M., Procter, J. B., Martin, D. M. A., Clamp, M., and Barton, G. J. (2009) Jalview Version 2: A multiple sequence alignment editor and analysis workbench. *Bioinformatics 25*, 1189−1191.
(43) Pettersen, E. F., Goddard, T. D., Huang, C. C., Couch, G. S., Greenblatt, D. M., Meng, E. C., and Ferrin, T. E. (2004) UCSF Chimera: A visualization system for exploratory research and analysis. *J. Comput. Chem. 25*, 1605−1612.
(44) Baker, N. A., Sept, D., Joseph, S., Holst, M. J., and McCammon, J. A. (2001) Electrostatics of nanosystems: Application to microtubules and the ribosome. *Proc. Natl. Acad. Sci. U.S.A. 98*, 10037−10041.
(45) Muhandiram, D. R., Guang, Y. X., and Kay, L. E. (1993) An enhanced-sensitivity pure absorption gradient 4D ^{15}N,^{13}C-edited NOESY experiment. *J. Biomol. NMR 3*, 463−470.